

See discussions, stats, and author profiles for this publication at: <http://www.researchgate.net/publication/268155227>

Molecular Dynamics Simulations of Complex Mixtures Aimed at the Preparation of Naproxen-Imprinted Xerogels

ARTICLE in JOURNAL OF CHEMICAL INFORMATION AND MODELING · NOVEMBER 2014

Impact Factor: 3.74 · DOI: 10.1021/ci5004575 · Source: PubMed

CITATION

1

READS

58

4 AUTHORS, INCLUDING:



Natália D. S. Cordeiro

University of Porto

242 PUBLICATIONS 2,845 CITATIONS

[SEE PROFILE](#)



Manuel Azenha

University of Porto

45 PUBLICATIONS 620 CITATIONS

[SEE PROFILE](#)

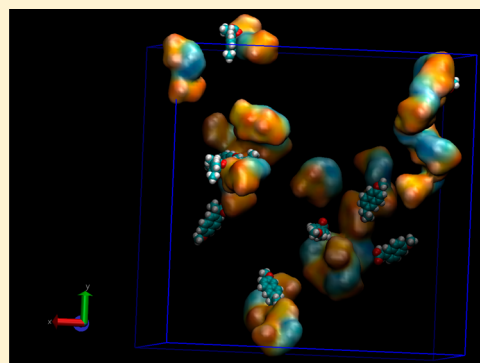
Molecular Dynamics Simulations of Complex Mixtures Aimed at the Preparation of Naproxen-Imprinted Xerogels

Riccardo Concu,^{*,†} Martin Perez,[†] M. Natália D. S. Cordeiro,^{*,†} and Manuel Azenha[‡]

[†]REQUIMTE and [‡]CIQ-UP, Department of Chemistry and Biochemistry, Faculty of Sciences, University of Porto, Rua do Campo Alegre 687, 4169-007 Porto, Portugal

 Supporting Information

ABSTRACT: The main objective of this study was to simulate for the first time a complex sol–gel system aimed at preparing the (*S*)-naproxen-imprinted xerogel with an explicit representation of all the ionic species at pH 9. For this purpose, a series of molecular dynamics (MD) simulations of different mixtures, including species never studied before using the OPLS-AA force field, were prepared. A new parametrization for these species was developed and found to be acceptable. Three different systems were simulated, representing two types of pregelification models: the first one represented the initial mixture after complete hydrolysis and condensation to cyclic trimers (model A); the second one corresponded to the same mixture after the evaporation process (model B); and the last one was a simpler initial mixture without an explicit representation of all of the imprinting-mixture constituents (model C). The comparison of systems A and C mainly served the purpose of evaluating whether an explicit representation of all of the components (model A) was needed or if a less computationally demanding system in which the alkaline forms of the silicate species were ignored (model C) would be sufficient. The results confirmed our hypothesis that an explicit representation of all of the imprinting-mixture constituents is essential to study the molecular imprinting process because a poor representation of the ionic species present in the mixture may lead to erroneous conclusions or lost information. In general, the radial distribution function (RDF) analysis and interaction energies demonstrated a high affinity of the template molecule, 2-(6-methoxynaphthalen-2-yl)propanoate (NAP⁻, the conjugate base of (*S*)-naproxen), for the gel backbone, especially targeting the units containing the dehydroimidazolium moiety used as a functional group. Model B, representing a nearly gelled sol where the density of silicates and solvent polarity were much higher relative to the other models, allowed for much faster simulations. That gave us the chance to observe the templating effect through a comparative analysis and observation of the trajectories from simulations with the template- versus non-template-containing mixtures. Overall, a strong coherence between the imprinting-relevant interactions, aggregation, or the silicate network texturing effects taken out of the simulations and the experimentally high imprinting performance and porosity features of the corresponding gels was achieved.



1. INTRODUCTION

In the past few years, the sol–gel polycondensation technique has been increasingly employed with great success as an alternative approach for the preparation of molecularly imprinted materials (MIMs).^{1–3} With this approach it is possible to prepare synthetic host systems bearing improved molecular selectivity.⁴ With respect to classical techniques, MIMs present several advantages such as physical robustness, long shelf life, simple preparation, great selectivity, etc. For these reasons, MIMs are being studied and used in very different fields such as solid-phase extraction, enantiomer separations, drug delivery, drug discovery, and ligand binding assays. These materials are often based on a silica backbone and inorganic–organic hybrid materials prepared with organically modified trialkoxysilanes (ORMOSILs). The most widely used precursors for preparing sol–gel materials have been silicon alkoxides, such as tetramethoxysilane (TMOS) or tetraethoxysilane (TEOS). Commonly, the imprinting protocols follow a co-polycondensation route between one of these precursors

and an ORMOSIL, R–Si(OR')₃ or (R'O)₃Si–R–Si(OR'')₃, where R represents an organic motif with affinity (usually via non-covalent interactions) for the template of imprinting. Upon hydrolysis and polycondensation of the precursor and the ORMOSIL, a hybrid organic–inorganic network is developed, where the [template–R motif] complexes are trapped upon gelification. Finally, removal of the template leaves a vacant recognition R site that has the ability to recognize the shape, size, and functionality of the template (or structurally related compounds). In Figure 1 we show a general scheme of the MIM process under study in the present work. It focuses on the dehydroimidazolium motif, a cationic ORMOSIL (Figure 2A) aimed at sol–gel molecular imprinting of NAP⁻, the carboxylate form of the nonsteroidal anti-inflammatory drug (*S*)-2-(6-methoxynaphthalen-2-yl)propanoic acid ((*S*)-naproxen) (Figure 2E). We have shown⁵ that highly selective sol–gel

Received: July 27, 2014



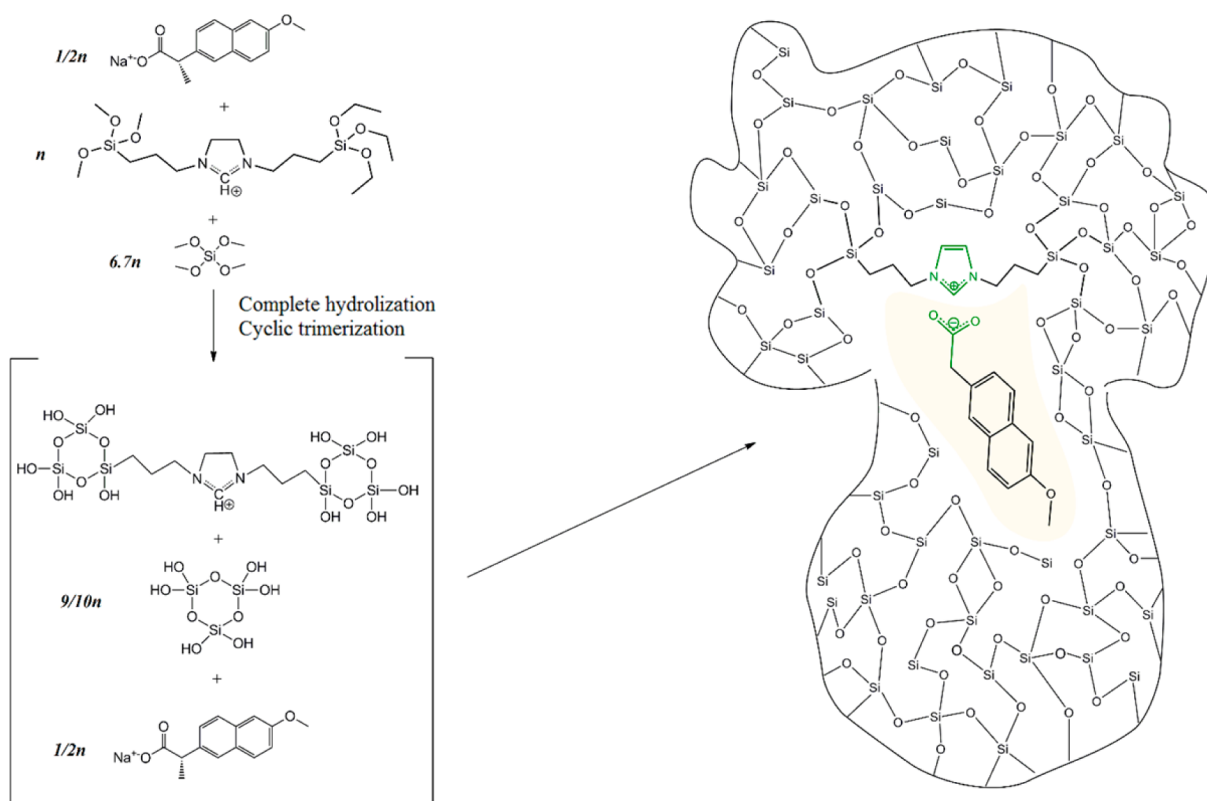


Figure 1. Scheme of the formation of a naproxen-imprinted xerogel obtained from a mixture of TMOS and AO-DHI⁺ iodide. The intermediate state shows the main species selected for the simulations, obtained after an idealized process of complete hydrolysis and cyclic trimerization. In the case of model A, the conjugate bases of the two silicate trimers (not shown) were also included, and the amount of solvent (25:1 methanol/water) reflected the initial experimental conditions. In model B, we kept the same numbers and natures of the silicated species and template as in model A, but the amount of solvent was much reduced (to ca. one-fifth that in A) and its proportion was changed to 5:1 methanol/water. It was intended here to study mixtures with characteristics of silicate density and solvent composition typical of a stage closer to the gelification. Model C was equivalent to model A with the difference that we did not include the conjugate bases of the shown cyclic trimers.

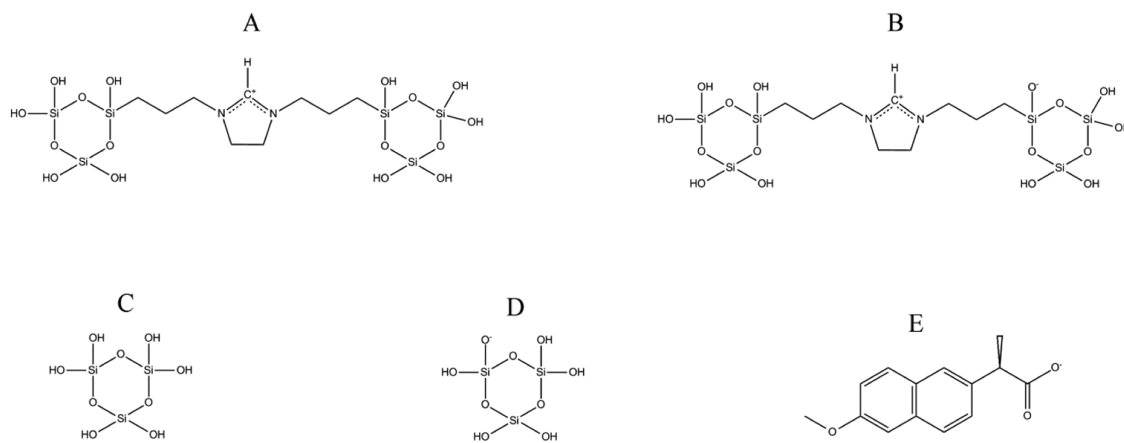


Figure 2. Molecular structures of (A) DHI⁺, (B) DHI^{+-/}, (C) SI3, (D) SI3⁻, and (E) NAP⁻.

naproxen imprints may be prepared by co-polycondensation of hydrolyzed TMOS and 1-(triethoxysilylpropyl)-3-(trimethoxysilylpropyl)-4,5-dihydroimidazolium iodide (AO-DHI⁺ iodide) in a water/methanol mixed solvent using NAP⁻ as the template. During those studies, several experimental observations raised questions whose answers were not straightforward. We could only appeal to our chemical intuition on the molecular-scale phenomena when it came to answering questions such as why the end-capped imprints were not so effective or why no enantioselectivity could be observed. We

believe that these and many other macroscopic observations related to the field of sol-gel molecular imprinting may be scrutinized via the application of computational chemistry techniques. In fact, we recently demonstrated for the first time the usefulness of molecular dynamics (MD) simulations of pregelification sol-gel mixtures^{6,7} to gain insight into the fine aspects of molecular interactions related to both the imprinting process and network structuring. Those MD simulations did not model the complex reactive mechanisms involved in the sol-gel process, a task that is too complex considering the

Table 1. Description of the Simulated Systems

model	methanol:water ratio	numbers of units of components							
		NAP ⁻	DHI ⁺	DHI ^{+/−}	SI3	SI3 ⁻	water	methanol	Na ⁺
A	25:1	10	10	10	9	9	310	7736	29
B	5:1	10	10	10	9	9	230	1130	29
C	25:1	10	20	—	18	—	310	7736	10

current computational resources. Nonreactive mixtures representing certain stages of the sol–gel process were thus considered as simplified approaches to the modeled systems. The mixtures contained water, methanol, damascenone (the imprinting molecule), Si₃O₃(OH)₆ (SI3) (Figure 2C) and, in some cases, Si₃O₃(OH)₅C₃H₆NHC₆H₅ (SIPA). SI3 and SIPA are three-silicate rings used as representatives for the initial small condensation products obtained from the polycondensation of three TMOS units (SI3) and the co-polycondensation of TMOS with the ORMOSIL (3-propylaminophenyl)-trimethoxysilane at a 6.7:1 molar ratio. We were conscious of such an oversimplification of the real sol–gel mixture and meant mainly to join together (respecting the experimental proportions) species regarded as providing a good resemblance to the final gel backbone (i.e., the same surface groups), the template, and the solvent medium. All of the components were neutral, since the simulations related to sol–gel synthesis were carried out at low pH values (below silica's isoelectric point, ~2). The simulations proved to be a useful tool for studying the solvation environment of the template and the silica clusters. The collected information about the competing interactions in different simulated systems corresponding to different experimental conditions was in excellent agreement with experimental observations of the performance of the prepared damascenone MIMs. Later, a similar study allowed us to ascertain the possible effects of adding poly(ethylene glycol) to the sol–gel mixtures used for the preparation of the damascenone imprints.³

Herein we present a study aimed at extending the applications of MD simulations to investigate the fine atomistic-level aspects related to the preparation of naproxen-imprinted hybrid silicas as described above. In this case, better imprinting performance was experimentally observed when NAP⁻, the sodium carboxylate derivative of naproxen, was employed as the template, and the sol–gel process took place at pH ~9. To be able to cope with such alkaline pH conditions, the MD simulations needed to incorporate a series of charged species, in agreement with the distributions predicted for the several species at that pH according to the acid–base equilibria involved. Moreover, the organic motif targeting the imprinting of NAP⁻ was a permanent cation of the (R'O)₃Si–R⁺–Si(OR")₃ type, a more complex structure than used before. Additionally, counteranions and cations were also needed in the system. Compared with the previous MD simulations, the present ones are of higher complexity and justify an effort to demonstrate the feasibility of MD under such “high charge density” conditions. This constitutes the main goal of the present research, which may be regarded as an intermediate but necessary stage before the envisaged application to more advanced simulations such as sol–gel/oil interfacial studies in the context of the emulsion preparation of imprinted silica micro- or nanospheres.

2. COMPUTATIONAL DETAILS

The MD simulations were performed with the GROMACS 4.5.5⁸ package applying the OPLS-AA⁹ force field, including the enhancements proposed by Price et al.¹⁷ for sol–gel reagents. GROMACS is an open-source software package that is widely used to perform MD simulations to simulate a great variety of systems; it has a good reputation concerning speed and reliability, in particular through the new GPU support, which is able to speed up an MD simulation up to 10 times. All of the systems under study contained water, methanol, the carboxylate form of (S)-naproxen (the template, NAP⁻), the dual cyclic silicate trimer corresponding to a hydrolyzed and condensed species derived from the cationic dehydroimidazolium ORMOSIL, [(Si₃O₃(OH)₅)C₃H₆]₂C₃H₅N₂⁺ (DHI⁺) (Figure 2A), and the silica trimer SI3. Depending on the case, some also contained DHI^{+/−}, the zwitterionic form obtained from DHI⁺ by the loss of a proton (Figure 2B), and also the anionic form of the silica trimer, Si₃O₃(OH)₅O⁻ (SI3⁻) (Figure 2D). All of the nonstandard parameters were described in a previous report,¹⁰ except those used for DHI⁺, DHI^{+/−}, and SI3⁻, which were parametrized for the first time in this work. The atomic point charges for the DHI⁺, DHI^{+/−} and SI3⁻ species were calculated using Gaussian 09¹¹ in an OPLS-AA-compliant manner, meaning that the geometry was first optimized at the HF/6-31G* level of theory and then partial charges were computed from a single-point run using the CHelpG scheme¹² at the B3LYP/6-311++G(2d,2p) level; information regarding these molecules is reported in the Supporting Information. This approximation was chosen over the standard OPLS-AA force field calculation (MP2/aug-cc-pVTZ//HF/6-31G*) because of the better stability of DHI⁺ and DHI^{+/−} when the 6-311++G(2d,2p) basis set was used. All of the studied models are summarized in Table 1. The numbers of functional silicate units (DHI⁺ plus DHI^{+/−}) and structural silicate units (SI3 plus SI3⁻) were determined from the experimental concentrations of AO-DHI⁺ iodide and TMOS. It was assumed that the precursors went through complete hydrolysis and fully condensed to DHI⁺ or SI3 (or its conjugate bases). On the other hand, the ratios of SI3 units to SI3⁻ units and DHI⁺ units to DHI^{+/−} units were estimated from a species distribution analysis conducted at pH 9 based on the acidity constant of the silanol group, keeping in mind that pK_a decreases by 1–2 units at high methanol contents.

For systems A and C, the initial state was obtained by inserting into the boxes the respective numbers of units at random positions using the packmol package.¹³ To obtain the initial state of the B system, we took the final state of the A system and removed a number of water and methanol molecules. This frame, after NpT ensemble equilibration, was set as the initial state of the B system (more details on this process will be given below). The initial box dimensions were estimated by considering the molecular weight and the density of each of the components of the mixture. After energy minimization using both the steepest-descent and L-BFGS

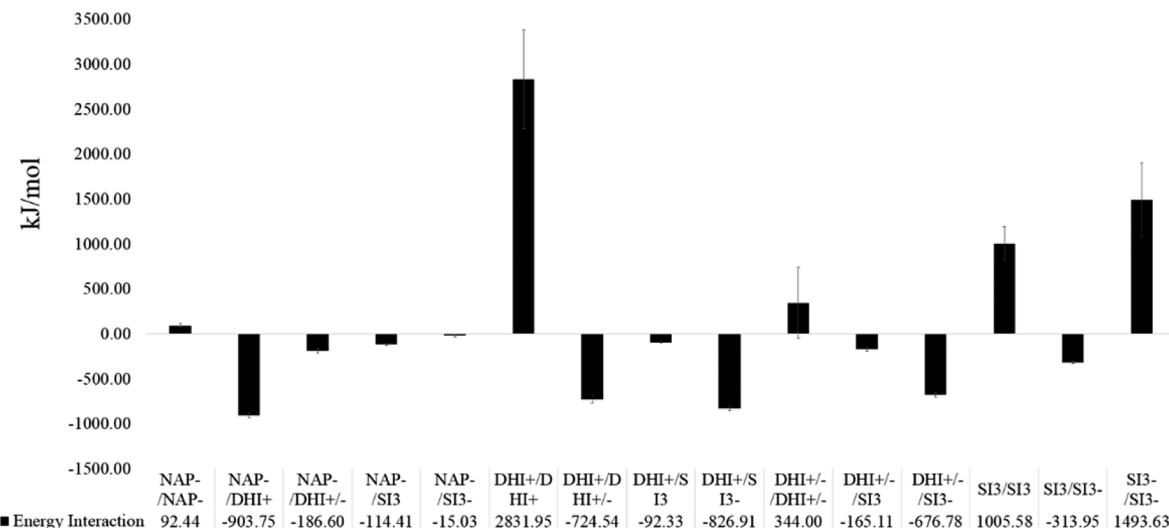


Figure 3. Interaction energies for the most important groups obtained in the SI3DHISI3:25:1 model.

methods included in the GROMACS package, temperature annealing was performed in the *NVT* ensemble for 1 ns, reaching a temperature of 600 K, in order to ensure proper mixing and gather three random independent initial configurations. These were subsequently used as starting configurations for the three independent MD equilibration runs needed to test the reproducibility of the simulations. Before the production stage, ~100 ns of simulation time in the *NpT* ensemble was used to equilibrate the system. As we expected, most of the intermolecular interactions reached stable values after 100 ns (plots of the energy are reported in Figure S10 in the Supporting Information), save for the largest groups present in the mixture (e.g., SI3^- , $\text{DHI}^{+/-}$, and DHI^+). Finally, production runs of 100 ns were performed in the *NpT* ensemble for data collection. Observable properties were sampled every 2 ps, from which total averages and standard deviations for each run were computed. The equations of motion were integrated using the Verlet leapfrog algorithm¹⁴ with a time step of 2 fs. Typically, the temperature (*T*) was kept fixed at 298 K by applying the velocity rescaling thermostat,¹⁵ and whenever necessary the pressure (*p*) was held constant at 1 bar using the Parrinello–Rahman scheme.^{16,17} The time constant used for the Parrinello–Rahman coupling was set to 1 ps. Periodic boundary conditions were applied in all three Cartesian directions. For the water molecules, the transferable intermolecular potential four-point (TIP4P) model¹⁸ was applied. The nonbonded electrostatic interactions were calculated using a sixth-order particle mesh Ewald (PME) method¹⁹ beyond a cutoff radius of 0.9 nm. The Lennard–Jones (LJ) potential was calculated within a cutoff radius of 0.9 nm with the help of a neighbor list that was updated every 10 time steps. A dielectric permittivity (ϵ_r) equal to 1 was used.

Statistical and trajectory analyses of the simulations were performed with the programs included in GROMACS, while visualizations were made with VMD.²⁰ The analysis essentially consisted of comparisons of the interaction energies between the relevant molecule and ion types; calculations of radial distribution functions (RDFs), coordination numbers (N_B), and diffusion coefficients (D); and clustering analysis. Both the interaction energy between two groups of molecules and the energy of interaction within the group were obtained as the simulation average of the sum of short-range LJ and Coulomb

energies. The RDF between different types of molecules was calculated as

$$g_{AB}(r) = \frac{\langle \rho_B(r) \rangle}{\langle \rho_B \rangle_{loc}}$$

where $\langle \rho_B(r) \rangle$ refers to the average density of particle B at a distance r around particle A and $\langle \rho_B \rangle_{loc}$ refers to the density of particle B averaged over all spheres around particle A within a maximum radius (r_{max}), which was half of the box length. The RDF was additionally averaged on all particles of type A present in the system and over the trajectory (simulation time). The g_rdf function included in the GROMACS package calculates the RDF in different ways. The normal method is around a (set of) particle(s), and the other methods are around the center of mass of a set of particles or to the closest particle in a set. Here the RDFs were calculated using the centers of mass of the particles by means of the mol_com option of g_rdf function included in the GROMACS package. The coordination number of a particle or atom B around a particle or atom A (N_B) was calculated by integrating the radial distribution function $g_{AB}(r)$ between the center of A and the first local minimum, r_m :

$$N_B = 4\pi\rho_B \int_0^{r_m} g_{AB}(r)r^2 dr$$

where ρ_B refers to the density of species B (expressed in units of molecules per unit volume). The cluster analysis was performed using the g_cluster package included in the GROMACS software. This utility can cluster structures using several different methods. We determined structures from the trajectories of the runs using the single linkage, which adds a structure to a cluster when its distance to any element of the cluster is less than the cutoff. We performed the cluster analysis using cutoff values (i.e., the largest distance to be considered in a cluster) between 0.3 and 1.50 nm. The diffusion coefficient of the mixture components was calculated from the Einstein relation (mean-square displacement, MSD):

$$D = \frac{1}{6t} \langle |\mathbf{r}_i(t) - \mathbf{r}_i(0)|^2 \rangle$$

where \mathbf{r}_i is the position of the center of mass of molecule i . The MSD was averaged over the molecules, and in order to improve

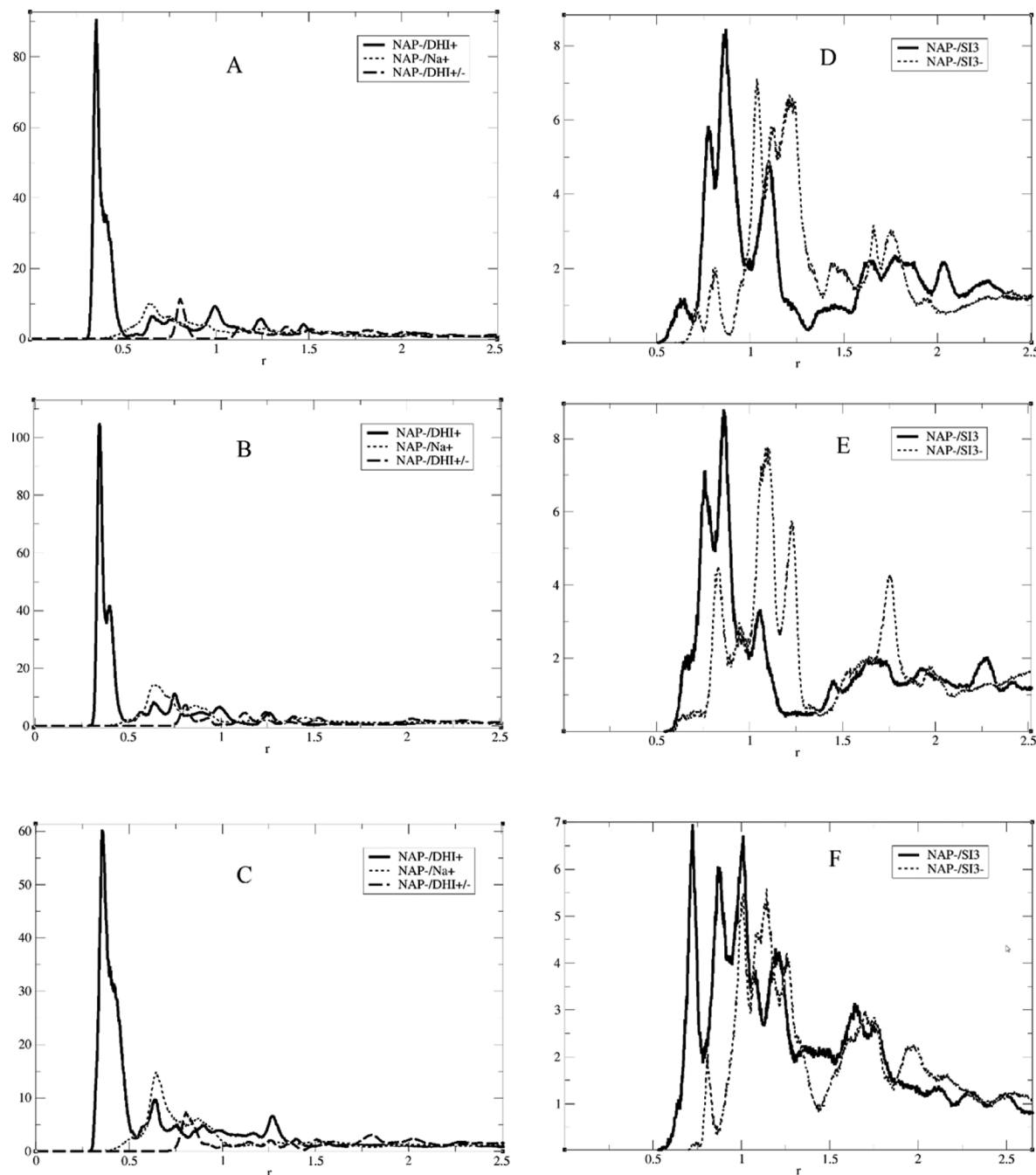


Figure 4. RDFs calculated from the trajectories of the three replicas of SI3DHISI3:25:1 run. A, B, and C are representative of the three replicas for group pairs NAP⁻/DHI⁺, NAP⁻/Na⁺, and NAP⁻/DHI^{+/-}. C, D, and E are representative of the three replicas for group pairs NAP⁻/SI3 and NAP⁻/SI3⁻.

the statistics, several restarts $r(0)$ were used along the trajectory.

3. RESULTS AND DISCUSSION

3.1. Foreword. In this work, we simulated a rather complex system comprising the new ionic compounds Si3⁻, DHI^{+/-}, and DHI⁺, which had never been modeled before using MD, together with cyclic oxysilane Si3, NAP⁻, Na⁺ and I⁻ counterions, and the solvents water and methanol. When the complexity and variety of species under consideration is increased, the probability of accumulating a significant amount of calculation errors and uncertainties is also increased.

Therefore, it was necessary to assess the validity of the potential considered for the simulations. The main limitation for doing it directly is that the real systems present a huge variety of oxysilane species at a certain moment of the process, making it really hard to perform exhaustive atomistic simulations to predict the experimental properties of a typical Si-based sol–gel process. For this reason, the experimental validation of the model had to be partially indirect. We chose the OPLS-AA potential including the fine-tuned parameters by Price et al.¹⁷ to better describe typical sol–gel reagents. First of all, the accuracy of the OPLS-AA potential has been extensively verified for small molecules such as water and methanol, so further testing was considered unnecessary for these substances.

Table 2. Coordination Numbers Calculated for Selected Groups in the Simulation

	A	B	C
NAP ⁻ /NAP	0.07	0.14	0.20
NAP ⁻ /DHI ⁺	0.20	0.21	0.10
NAP ⁻ /DHI ^{+/-}	0.11	0.26	—
NAP ⁻ /SI3	0.04	0.66	0.09
NAP ⁻ /SI3 ⁻	0.01	0.05	—
NAP ⁻ /Na ⁺	0.74	0.65	—
SI3/DHI ⁺	0.11	0.09	0.05
SI3/DHI ^{+/-}	0.11	0.16	—
SI3/SI3	0.59	0.43	0.11
SI3/SI3 ⁻	0.33	0.24	—
DHI ⁺ /DHI ⁺	0.16	0.38	0.79
DHI ⁺ /DHI ^{+/-}	0.10	0.49	—

This potential was previously studied by our group⁶ for cyclic SI3 in a mixture that included damascenone, TMOS, water, and

methanol. In that work, the calculated volumetric mass densities of the different species considered were in good agreement with experimental data, the difference in all cases being equal to or less than 6.8% (worse case for TMOS).

The cationic ORMSIL derivative (in the forms DHI^{+/-} and DHI⁺) is perhaps the most difficult molecule to simulate in our systems because of the presence at the same time of oxysilane rings, the dehydroimidazolium cationic moiety, and additional permanent charges. DHI⁺ is the less-investigated structure in our system, and its modeling and validation will be explained more in detail. To compare the simulation results with experimental data, the ORMSIL precursor AO-DHI⁺ iodide was synthesized and characterized. The difference between the synthesized cation AO-DHI⁺ and DHI⁺ is the substitution of triethoxysilane and trimethoxysilane by SI3 moieties, obtainable after the aforementioned idealized hydrolysis and condensation process. Since both methoxysilane and ethoxysilane parametrizations have been previously validated, a good agreement between the experimental and simulated densities would

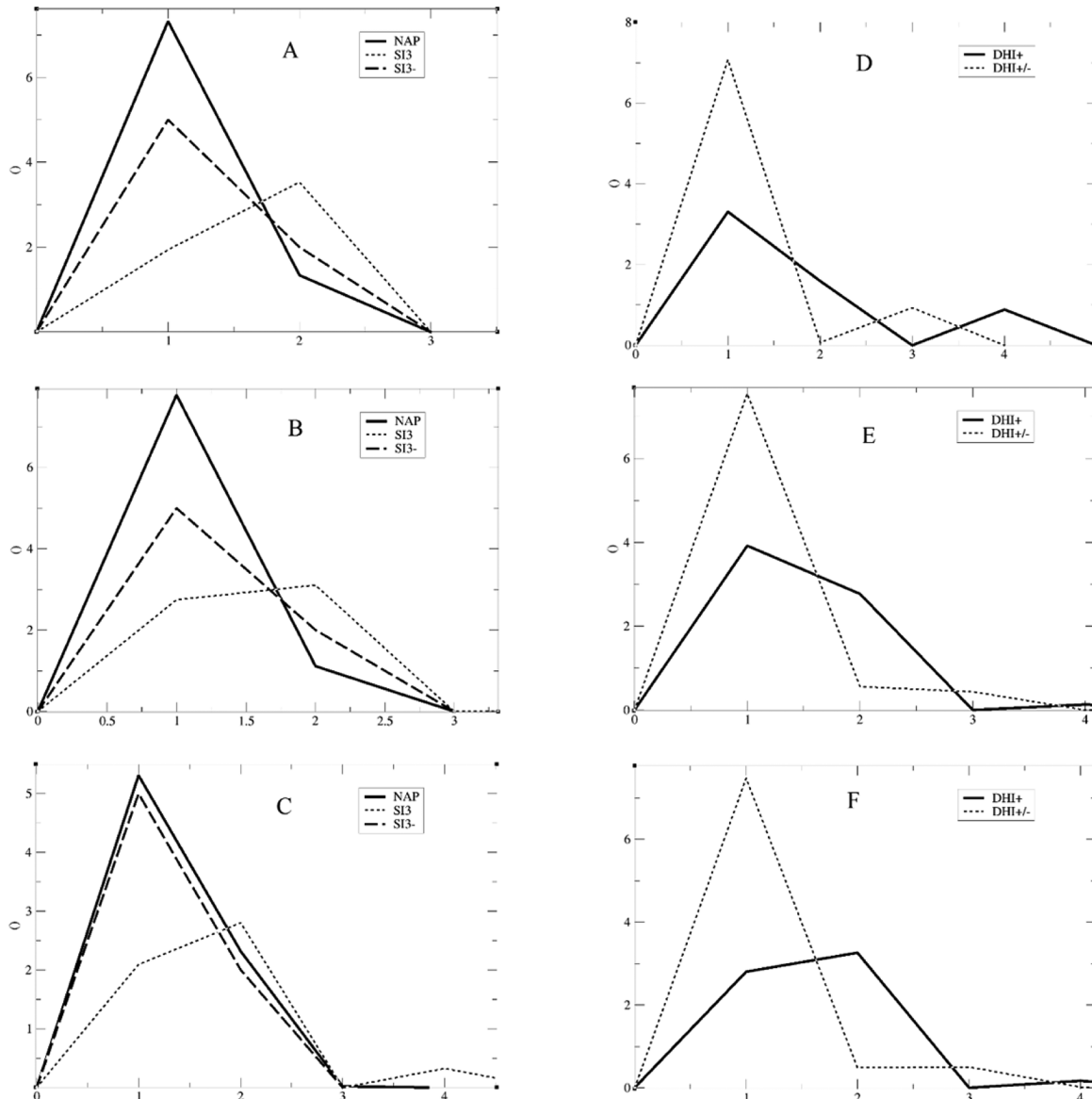


Figure 5. Cluster analyses of (A–C) SI3, NAP, and SI3⁻ and (D–F) DHI⁺ and DHI^{+/-} calculated from the trajectories of the SI3DHISI3:25:1 runs. Each image is representative of one replica.

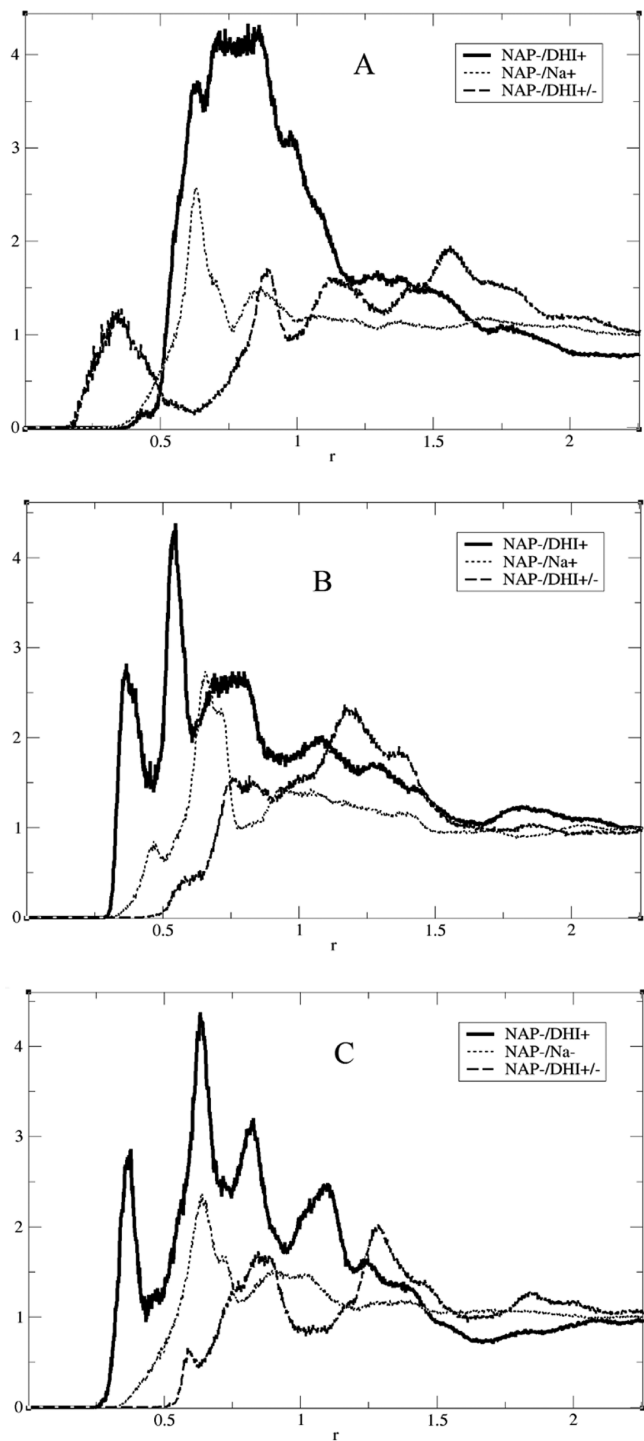


Figure 6. RDFs calculated from the trajectories of the SI3DHISI3:2.5:1 run for the atom-type pairs NAP⁻/DHI⁺, NAP⁻/DHI^{+/-}, and NAP⁻/Na⁺.

provide a satisfactory indication of the adequate parametrization used for the DHI⁺ substructure. For the simulations, a pure AO-DHI⁺ iodide system consisting of 500 ion pairs in a cubic box was considered. The density of the ionic liquid measured in the laboratory was $1180 \pm 40 \text{ kg/m}^3$ at 298 K, while the density calculated by MD was $1260 \pm 1 \text{ kg/m}^3$. This is a non-negligible difference (6%), but it is below the value of 6.8% previously cited. Therefore, we concluded that the model is reasonably good considering the complexity of the molecule, the potential

impurities in the experimental sample (which are not present in the simulated one), and the inherent limitations of the MD approximation.

The calculation of diffusion is not straightforward because it is very sensitive to modeling conditions such as the force field, time step, and NpT algorithm.²¹ Generally speaking, the analysis of the diffusion and the trajectories of the simulations described in the next sections reveal a clear precolloidal character of the mixtures, expressed by the presence of large aggregates of the silicate species (SI3, SI3⁻, DHI⁺, and DHI^{+/-}) characterized by a very low mobility ($(0.004\text{--}0.02) \times 10^{-5} \text{ cm}^2/\text{s}$) compared with the solvent molecules ($(0.2\text{--}0.9) \times 10^{-5} \text{ cm}^2/\text{s}$). The values of the diffusion coefficients are reported in Table S5 and Figures S7–S9 in the Supporting Information. This behavior was expected and yet reported by other authors²² for the SI3 species alone.

3.2. Model A. As depicted in Figure 1, model A corresponds to the hypothetical intermediate stage reached by the complete hydrolysis of the initial precursors and the formation of the SI3 and DHI⁺ condensates and their conjugate bases SI3⁻ and DHI^{+/-} in accordance with the initial experimental concentrations and solvent composition⁵ (cf. Table 1). As previously mentioned, we performed three independent runs for each system. In the case of model A, the template molecule exhibited an impressive affinity for DHI⁺ and a very good one for DHI^{+/-}. In fact, the analysis of the intermolecular interactions occurring during the simulation clearly shows that major interactions occur between the group pairs DHI⁺/NAP⁻, DHI⁺/SI3⁻ and DHI⁺/DHI^{+/-}, as reported in Figure 3. As expected, the most unfavorable interaction during the simulation was between the DHI⁺ groups (+2831 kJ/mol), whereas the most favorable interaction energy was recorded for the DHI⁺/NAP⁻ pairs (-903 kJ/mol), thus indicating a great affinity between this latter pair. Regarding the other groups, it is important to underline the favorable SI3⁻/SI3 interaction (-313 kJ/mol) and the unfavorable energy for the SI3⁻/SI3⁻ pair (+1493 kJ/mol). In addition, is important to underline the good affinity of DHI⁺ and DHI^{+/-} for SI3⁻ (-826 and -676 kJ/mol, respectively). This is a relevant result because it points to an interconnecting trend that leads to the co-polycondensation of the different silicate units in the mixture, thus driving the system toward the formation of a homogeneous backbone. These results are in agreement with the RDFs. Indeed, from analysis and comparison of the graphs for this calculation, the high affinities of the template molecule for DHI⁺ and for DHI^{+/-} are notable, as reported in Figure 4A. The sharp, high peak for the NAP⁻/DHI⁺ pair at 0.4 nm clearly shows that the template affinity for the xerogel is optimal. On the other hand, the template molecule shows a very low preference for the counterion, as reported in Figure 3. These results are further confirmed by the N_B analysis, which clearly shows the preference of the template molecule for the DHI⁺ and DHI^{+/-} groups, as reported in Table 2. In regard to N_B , it is important to underline that this number is calculated using the RDF first global minimum. Thus, it is strictly correlated to the distance in which the minimum is located. In our case, the NAP⁻/DHI⁺ pair has a mean N_B value of 0.2, but the minimum is at a very close distance (0.5 nm) whereas, for example, the coordination number for the NAP⁻/Na⁺ pair is 0.7 but it was calculated at a distance of 1.2 nm. Hence, the highest coordination number does not obviously mean better affinity. Moreover, in all of the runs, the template does not exhibit appreciable affinity for SI3 and SI3⁻, and in fact the RDF

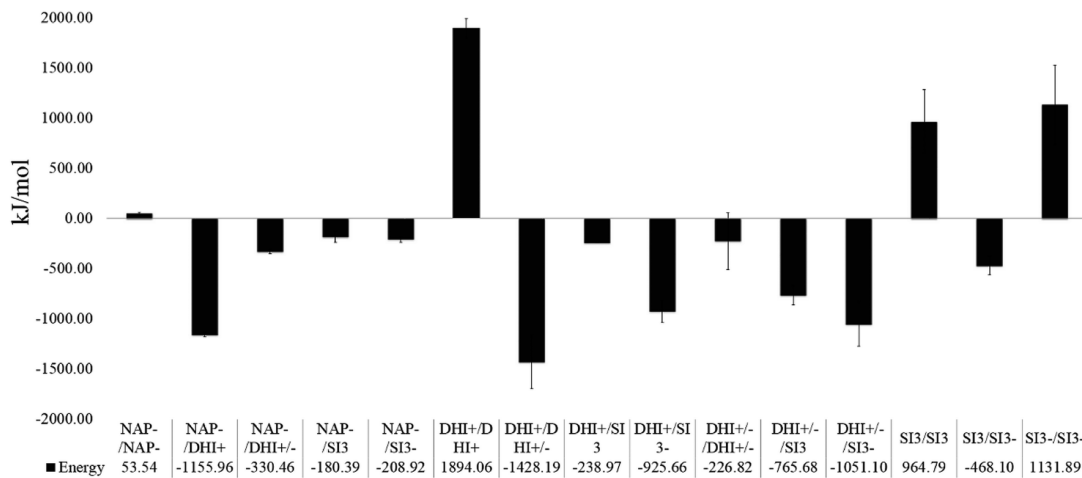


Figure 7. Interaction energies for the most important groups obtained in the SI3DHISI3:5:1 model.

analysis shows very low peaks at a greater distance (0.8 nm) compared with NAP/DHI⁺, as reported in Figure 4D. SI3 shows a great affinity for itself and for SI3⁻, and in fact the RDF in Figure 3 reveals a very high, sharp peak for the SI3/SI3⁻ pair at 0.6 nm. In addition, the peaks for the SI3/SI3⁻ and SI3⁻/SI3⁻ pairs are high, remarking the good affinities between these groups. As expected, N_B is in agreement, with mean values of ~0.6 and ~0.3 for SI3/SI3 and SI3/SI3⁻ pairs, respectively. All of these results are in agreement with previous work,²² where the trend of SI3 to form aggregates was reported. The trend of SI3 and SI3⁻ to form clusters is confirmed by our simulations; the typical cluster of SI3 in this simulation is normally formed by two molecules and along the simulations the number of clusters is usually 3, as depicted in Figure 5. DHI⁺ and DHI^{+/-} show a general trend to form small aggregates of 2 and 4 units (Figure 5D–F), thus indicating that the backbone may potentially grow and the building blocks tend to interact, which is expected during the sol–gel process.

Overall, the results presented are compatible with a successful imprinting process. In fact, during the entire simulation time (100 ns) the template molecules remained near the silica aggregates, mostly those containing the dehydroimidazolium group, which constitutes the most favorable scenario leading to an effective imprinting process. Of course, that does not represent a direct evaluation of the quality of the simulations, but unfortunately, the real mixtures are even more complex and it would not be feasible to isolate experimentally any of the calculated parameters. It is only possible at the moment to highlight the consistency between the simulation results and the final imprinting efficiency observed experimentally. In this regard, the model B simulations (discussed in the following), either with template or without template inclusion (nonimprinting mixture) led us to conditions relatable to nearly gelled mixtures, where an additional type of indirect evaluation of the simulations could be made.

Another reason for moving to model B (and also C) concerns the very high computational demand (2 ns/day) of model A, since the system was composed of a very large number of units (>8000). In view of even more demanding biphasic future simulations, models B and C would represent significant savings due to removal of ca. four-fifths of the solvent molecules in model B and the reduction in the number of charged units in model C. In addition, in our opinion, these

large systems in the near future could be simulated using a coarse-graining methodology²³ and/or with GPU-based computing,²⁴ but it is essential to previously simulate the system at an atomistic level in order to gain a better knowledge of the mechanisms regulating these systems.

3.3. Model B. Experimentally, the mixtures represented by the previous model may take a very long time to gel (days or weeks). One common way to speed up the process is by allowing slow evaporation of the solvent. Model B was built according to that experimental practice. The same number of units as in model A was kept, except that a number of methanol and water molecules were removed. To roughly estimate the number of water and methanol molecules remaining after this process, the vapor pressures of water (3.2 kPa) and methanol (17.0 kPa) at 298 K, the respective mole fractions in the mixture, and Raoult's law were considered, and a stepwise batch evaporation model was also applied. Basically, a methanol loss of 85% was considered to be achieved in five equalitarian steps. Step 1 consisted of an estimation of how much water would be lost based on the initial mole fractions and evaporation of one-fifth of the methanol. In step 2, with the mole fractions recalculated after step 1 and evaporation of two-fifths of the methanol, a second water loss estimation was obtained, and so on.

The new model was much less demanding in terms of computation load (<1500 units, 20 ns/day), and the volume of the simulation boxes was reduced from ~81 to ~47 nm³. Model B could thus easily solve the problem of computational effort required by model A. Although the condensed silicate species remain the same, this new model may also be regarded as describing the sol–gel mixture in a later stage of the sol–gel process that corresponds to a step closer to the gelification point. Here the aggregation level between the silicates would expectedly be much higher, and at the same time the solvent would be more polar (more water-rich). Therefore, this model was considered as providing different but equally useful information. At a glance, the removal of solvent indeed heavily affected the behavior of the system, exhibiting important changes. In general, the RDFs confirm the trends reported for model A, but the three replicas are not as similar as those reported for model A. In fact, the template molecule still has better affinity for DHI⁺ but shows an increasing affinity for DHI^{+/-} and Na⁺, as can be seen in Figure 6. Some of the RDFs differ significantly from run to run, but in any case, the template

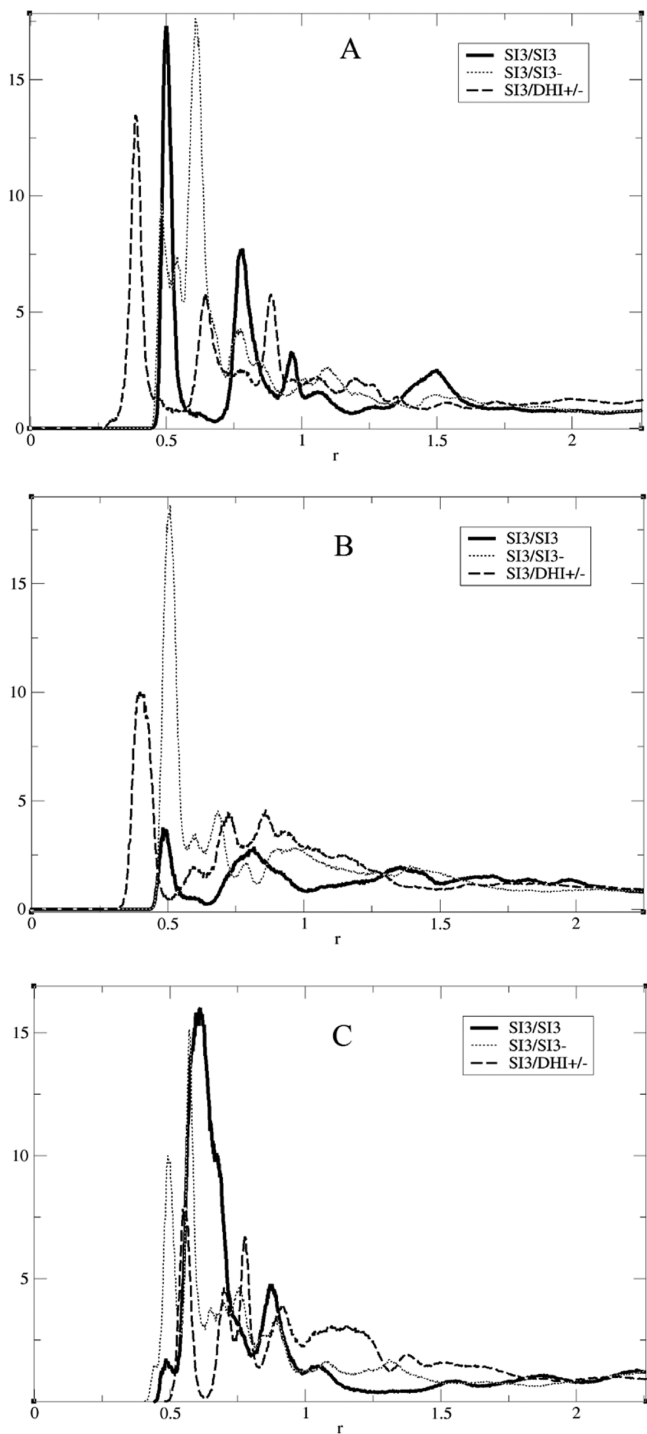


Figure 8. RDFs calculated from the trajectories of the SI3DHISI3:25:1 run for the atom-type pairs SI3/SI3, SI3/SI3⁻, SI3/DHI^{+/-}.

molecule still presents a preferred affinity for the DHI⁺ species, confirming the trend shown in system A. In the case of the first replica (Figure 6A), for the NAP⁻/DHI⁺ pair we have a peak at 0.6 nm very close to a maximum at 0.75 nm characterized by a large plateau. In the same figure, the RDF of the NAP⁻/Na⁺ pair shows a lower peak at 0.6 nm, underlying a growing affinity between these two pairs. This is the most important difference between this system and system A. For the NAP⁻/DHI^{+/-} pair we recorded the first peak at 0.3 nm, but in this case the affinity was lower compared with the other groups. In the other two replicas (Figure 6B,C), the RDFs of NAP⁻/DHI⁺, NAP⁻/Na⁺,

and NAP⁻/DHI^{+/-} present similar behaviors. In fact, the RDF of NAP⁻/DHI⁺ exhibits two peaks, the first one at 0.4 nm and the second one, very sharp, at 0.6 nm pointing out the good affinity between these two groups and thus agreeing with an effective imprinting of the template molecule on the backbone. As in the first replica, the RDF of NAP⁻/Na⁺ presents a well-defined peak at 0.65 nm remarking the change in the affinity between the template and its counterion. In regard to the NAP⁻/DHI^{+/-} pair, the first peak with a small plateau at 0.7 nm was recorded, highlighting a low affinity for this pair, as in the other replicas. These data are in agreement with the coordination number, where the same behavior as in system A was observed, but with a stronger interaction between the template and DHI^{+/-}, as reported in Table 2. Consistently, the coordination number for the NAP⁻/DHI⁺ and NAP⁻/DHI^{+/-} pairs is ~ 0.2 , denoting a general good affinity between the template and these two species, as previously shown by the RDFs, while that for the NAP⁻/Na⁺ pair is ~ 0.6 , as expected considering the RDF analysis. This growing affinity could be explained by the lower affinity of the template for DHI⁺. We have to underline here that for these two pairs the coordination number was calculated at a greater distance than for the NAP⁻/DHI⁺, and thus, it is normal that their values are higher.

In agreement with these data, the interaction energies between the template and DHI⁺/DHI^{+/-} are considerably increased to -1155 and -330 kJ/mol, respectively. In addition, the pairs DHI⁺/DHI^{+/-}, DHI⁺/SI3⁻, DHI^{+/-}/SI3⁻, and DHI^{+/-}/SI3 show growing interaction energies, with values of -1428 , -925 , -1051 , and -765 kJ/mol, respectively, as shown in Figure 7. The growing affinities between this species and DHI^{+/-}, SI3, and SI3⁻ mean that the backbone continues its trend to grow homogeneously, as we should expect to be the case in a real system. On the other side, the DHI⁺/DHI⁺ pair is the group with the most unfavorable energy, $+1894$ kJ/mol, followed by SI3⁻/SI3⁻, $+1131$ kJ/mol, and SI3/SI3, $+964$ kJ/mol. Regarding the pair SI3/SI3⁻, in this case we have recorded the most favorable interaction between these molecules, -468 kJ/mol, which is reflected in the RDF, as reported in Figure 8. It can be seen that there is a low variability between the three replicas. In fact, in the first replica (Figure 8A), a high, sharp peak for each group pair is present in the graph; it is notable that the SI3/DHI^{+/-} pair has a peak at a very close distance of 0.4 nm, while the peak for the SI3/SI3 pair is present at 0.5 nm and that for the SI3/SI3⁻ pair at 0.6 nm, but these later are higher than the former. In the second replica, the pair groups have the peaks at the same distances but the heights are very different: the SI3/SI3⁻ peak is the highest, while it is notable that the SI3/SI3 peak is the lowest. In the third replica, the SI3/SI3 peak is the highest, while the SI3/DHI^{+/-} is the lowest. These changes are reflected by the coordination number (Table 2), which shows a notable drop of affinity for the SI3/SI3 pair and a slight drop for the SI3/SI3⁻ pair. Consistently, the cluster analysis shows a higher propensity of SI3 and SI3⁻ to form large aggregates, confirming the general trend for these units as reported in Figure 9A-C. The cluster analysis also reveals that DHI⁺ and DHI^{+/-} in this system form very large aggregates (Figure 9D-F). This fact is really relevant because it endorses the other result we obtained, highlighting that this simulation is capable of reproducing the behavior of this sol-gel system at a stage closer to gelification where a large and homogeneous backbone is presented. This, together with the affinity of the template for the DHI monomers, is really indicative of an effective imprinting effect of NAP⁻ on the backbone. All of

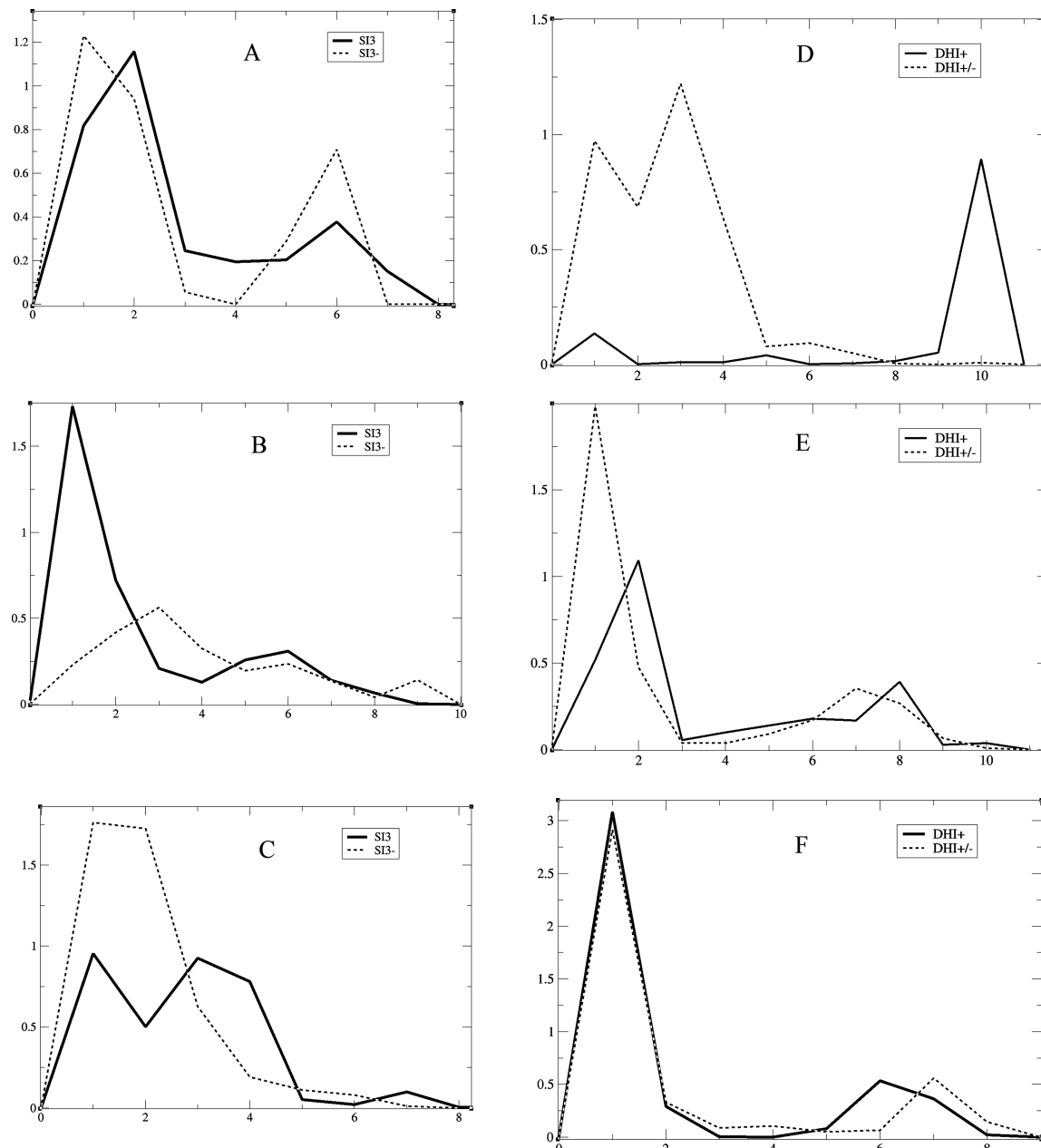


Figure 9. Cluster analyses of (A–C) SI3 and SI3[−] and (D–F) DHI⁺ and DHI^{+/−} calculated from the trajectories of the SI3DHISI3:5:1 runs. Each image is representative of one replica.

these results are supported by the coordination number of the SI3/SI3 pair, with mean values of ~ 0.4 for SI3/SI3 and 0.2 for SI3/SI3[−]. In regard to the DHI monomers, N_B confirms the precedent results with a notable increase compared with model A; in fact, we have recorded values of 0.4 for the DHI⁺/DHI⁺ pair and 0.5 for the DHI⁺/DHI^{+/−} pair, as can be seen in Table 2.

Given the relatively low computational demand of model B, we decided to simulate also a variant of this model (model B-NI) consisting on the simple removal of the template (NAP[−]), representing thus a model of the mixture for the preparation of the nonimprinted xerogel, a reference material routinely prepared experimentally for ascertaining the imprinting effect. The comparative analysis of the interaction energies (Table S6 in the Supporting Information) and the side-by-side presentation of snapshots taken from the trajectories of the

simulations of models B and B-NI (Figure S6 in the Supporting Information) are quite elucidative of the effect of the presence of the template. The snapshots clearly evidence the structuring effect of the template on the silicate aggregates, substantiated by a dispersive action. The presence of the template, bearing good affinity with the gel backbone, implies a real interposition between the network-forming units, leading to a much less compact structure that is able to accommodate the template. The values of the interaction energies corroborated such a dispersive modulating effect by the template. Indeed, globally it was observed that the presence of the template impeded a higher level of interaction between the network-forming units, as occurred within the nontemplated mixture. Such a textural effect of the naproxen template must translate into the porosity features of the final xerogel, and accordingly, the Brunauer–Emmett–Teller N₂ adsorption analysis of the experimental

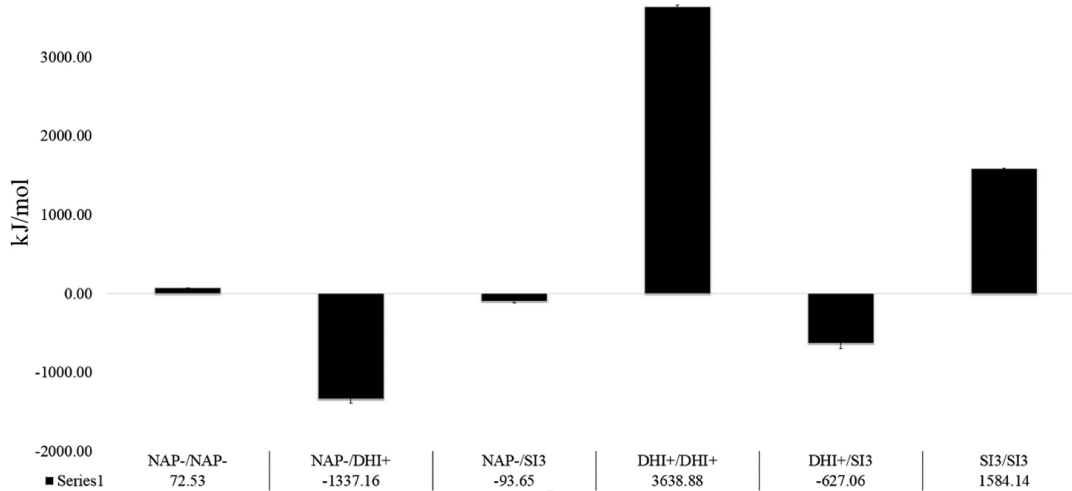


Figure 10. Interaction energies for the most important groups obtained in the SI3:25:1 model.

counterparts of models B and B–NI showed⁵ that although both materials presented very small pore volumes (imprinted 0.0038 mL/g vs nonimprinted 0.0013 mL/g), the imprinted material presented a significantly higher porosity.

The results obtained with these models are thus compatible with the behavior of mixtures that led to successfully imprinted xerogels, indicating that this kind of simulation can be useful in the study of such systems, at least in qualitative terms. The comparison of the templated versus nontemplated mixtures showed the expected templating effect, in agreement with the RDF analysis and N_B computation. Thus, in our opinion this kind of approach has the potential to be used to prepare models of nearly gelled imprinted gels that could be used to evaluate the recognition properties of a molecularly imprinted polymer against a non-imprinted one.

3.4. Model C. The last simulated model was built to compare the behavior of the system in the absence/reduction of some ionic species, which lowers the computational demand compared with that required by model A, in this case by reducing the number of charged species. This system was built using the same number of molecules of water and methanol as in model A but did not include the SI3^- and $\text{DHI}^{+/-}$ species. In other words, we wanted to ascertain whether the acid–base equilibrium of silanol could be suppressed without implicating erroneous conclusions or losing some important information. In order to respect the same stoichiometry as in model A, the system comprised 20 molecules of DHI^+ and 18 of SI3 , as reported in Table 1. As for the other systems, we performed the analysis of the intermolecular interactions. Again, the $\text{NAP}^-/\text{DHI}^+$ pair had the most favorable interaction energy, -1337 kJ/mol, clearly showing the good interaction for this pair. In addition, the good affinity between the $\text{DHI}^+/\text{SI3}$ pair, with a favorable interaction energy of -627 kJ/mol, is remarkable. On the other hand, the $\text{DHI}^+/\text{DHI}^+$ pair is the group with the most unfavorable interaction energy, followed by the pair $\text{SI3}/\text{SI3}$ ($+3638$ and $+1584$ kJ/mol, respectively; Figure 10). Another important consideration when comparing the interaction energies of the three simulated models is that in this case the standard deviation along the three simulations is the lowest because of the reduced number of charged species present in the box. Consistent with the energies, the RDF analysis revealed that NAP^- still has a good affinity for DHI^+ but at the same time has a better association for its counterion present in

the system (Na^+), as reported in Figure 11A. This change could not be totally unexpected because in this system DHI^+ cannot easily interact with its anionic counterpart ($\text{DHI}^{+/-}$) as a result of the absence of the anionic charge. Thus, in this system the silicate species form a smaller and less homogeneous backbone that is more disperse. Hence, Na^+ and NAP^- can better diffuse thorough the solvent and interact with each other. In the case of DHI^+ , the simulation shows a decrease in affinity for the template and a growing affinity for SI3 , as reported in Figure 11B. These changes are induced by the growth in the affinity of NAP^- for Na^+ . Furthermore, analysis of the trajectories and the cluster analysis confirms the trend of SI3 to form large aggregates; in fact, the cluster analysis along the three replicas shows a clear trend of SI3 to form clusters formed by four or five monomers, as reported in Figure 12. This result is endorsed by the RDF analysis, which reveals that SI3 has a great affinity for itself and an increased affinity for DHI^+ (Figure 11B). In view of all these data, it is remarkable that the template molecule still has a good affinity for DHI^+ , highlighting also in this simulation the favorable interactions that lead toward an effective imprinting of the template molecule on the silica backbone. In qualitative terms, this model allowed us to reach similar trends for the most relevant interactions concerned with the imprinting process (template–template, template–functional silicates, template–structural silicates, and functional silicates–structural silicates). However, the gain in computational performance in the absence of $\text{DHI}^{+/-}$ and SI3^- was not that significant (2 ns/day for system A vs 4 ns/day for system B). In addition and more important, the results of this model compared to system A clearly reveal that an explicit representation of the ionic species is essential to study and understand the behavior of such a complex system. In fact, because of the absence of $\text{DHI}^{+/-}$ in this system, it was impossible to evaluate whether a polycondensation trend occurring between major species (DHI^+ , $\text{DHI}^{+/-}$, SI3 , and SI3^-) is present. In this context, it is preferable to simulate a system with a major number of species in order to gain also an understanding of the mechanisms that may involve all of the possible charged species. With these results in mind, we thought that it was not necessary to simulate system B with the same approximation we used in going from system A to system C, since there would not be a significant speed-up of the

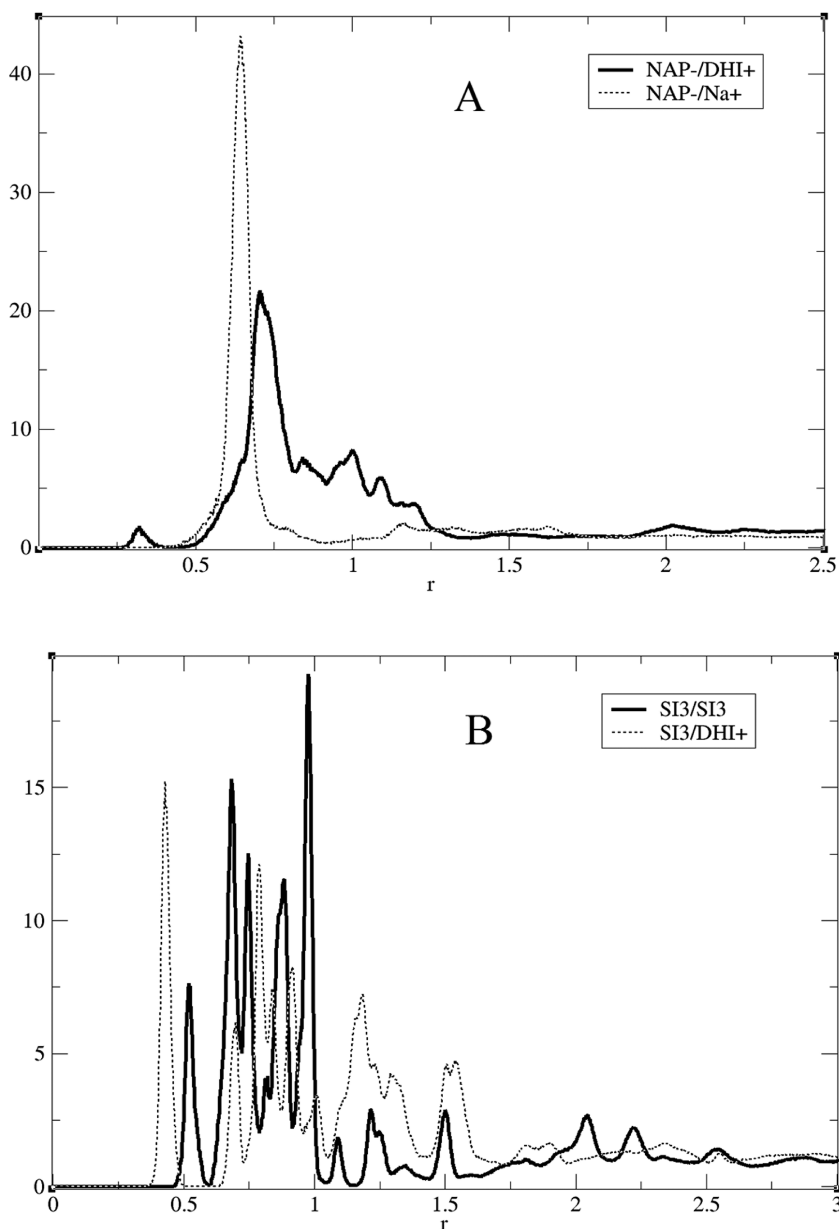


Figure 11. RDFs calculated from the SI3:25:1 run.

simulations and, on the other hand, important loss of information may occur.

4. CONCLUSIONS

This paper represents a significant step forward for future studies of the molecular imprinting process in a sol–gel system through atomistic MD simulations. It is important to underline that MD simulations can provide molecular-level details and uncover the atomistic basis of the interaction between the xerogel and the template molecule. The simulated systems were rather complex and included a new functional silicate in its cationic and zwitterionic forms (DHI^+ and $\text{DHI}^{+/-}$) and the anionic form of the well-studied SI3 (SI3^-). In this context, the main objective of this paper was to study of the affinity of $\text{DHI}^+/\text{DHI}^{+/-}$ for (*S*)-naproxen, the template molecule. For the first time, these new silicates have been simulated in a series of atomistic MD simulations with an explicit representation of all of the ionic species according to the pH of the system; in

this sense, the physical plausibility of the parametrization of the new molecules (to the OPLS-AA force field) was successfully checked in order to assess the reliability of the systems and simulations. The analyses of the simulations by means of RDFs, N_B values, and interaction energies of the groups have demonstrated the high affinity of the xerogel for the template molecule even after loss of solvent (model B). In this sense, the model A was the most representative in providing the clear imprinting effect of the template molecule on the xerogel; thus, all of the results obtained clearly show that (*S*)-naproxen has a great affinity for DHI^+ and a good affinity for $\text{DHI}^{+/-}$. In model B, with a much higher density of silicate units and other conditions resembling a nearly gelled sol, the imprinting effect was not so marked, but the association between NAP^- and DHI^+ was always the highest compared with other groups. This model allowed us also to observe a clear texturing dispersive effect of the template on the silicate network in order to be accommodated within that network. This result was no less

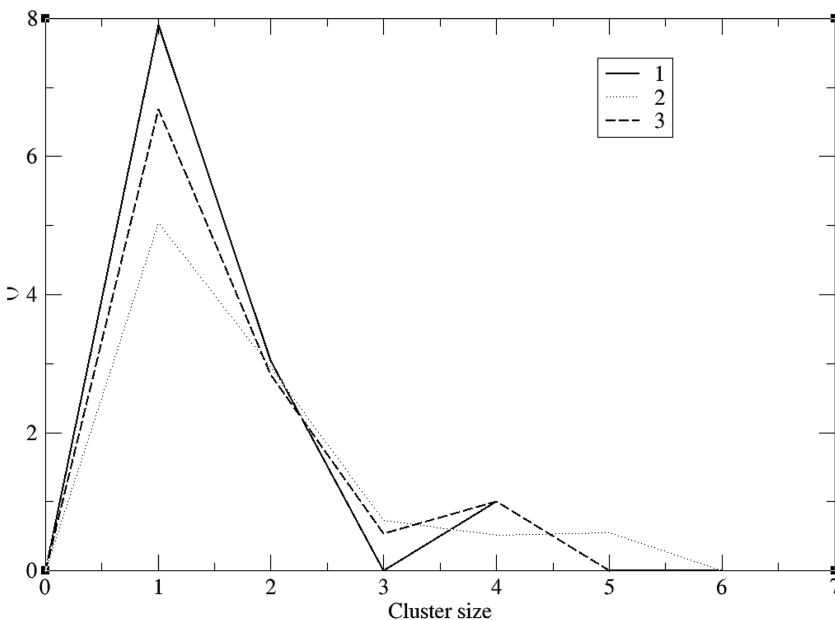


Figure 12. Cluster analysis of the SI3 molecule; 1, 2, and 3 are the replica numbers.

than testifying that the process of molecular imprinting was taking place. Finally, it is important to notice that although the results of the simulations could not be validated directly against any property measured experimentally, the scenarios observed by MD, especially for model B, were totally consistent with the behavior observed for the materials prepared in the lab, namely, a good imprinting effect as ascertained by an imprinted/nonimprinted adsorption and porosity comparison.

■ ASSOCIATED CONTENT

S Supporting Information

Atomic point charges and geometries used for the DHI⁺, DHI⁺⁻, and SI3⁻ molecules. This material is available free of charge via the Internet at <http://pubs.acs.org>.

■ AUTHOR INFORMATION

Corresponding Authors

*E-mail: ric.concu@gmail.com.

*E-mail: ncordeir@fc.up.pt.

Notes

The authors declare no competing financial interest.

■ ACKNOWLEDGMENTS

This work received financial support from the European Union (FEDER funds through COMPETE) and National Funds (FCT, Fundação para a Ciência e a Tecnologia) through Projects Pest-C/EQB/LA0006/2013 (REQUIMTE) and Pest-C/QUI/UI0081/2013 (CIQ). The work also received financial support from the European Union (FEDER funds) under the framework of QREN through Project NORTE-07-0124-FEDER-000067-NANOCHEMISTRY. R.C. also acknowledges FCT and the European Social Fund for financial support (Grant SFRH/BPD/80605/2011). The authors are greatly indebted to all of the financing sources.

■ REFERENCES

- (1) Collinson, M. M. Sol–Gel Strategies for the Preparation of Selective Materials for Chemical Analysis. *Crit. Rev. Anal. Chem.* **1999**, 29 (4), 289–311.

(2) Zhang, H.; Ye, L.; Mosbach, K. Non-covalent molecular imprinting with emphasis on its application in separation and drug development. *J. Mol. Recognit.* **2006**, 19 (4), 248–259.

(3) Díaz-García, M. E.; Laínño, R. B. Molecular Imprinting in Sol–Gel Materials: Recent Developments and Applications. *Microchim. Acta* **2005**, 149 (1–2), 19–36.

(4) Vasapollo, G.; Sole, R. D.; Mergola, L.; Lazzoi, M. R.; Scardino, A.; Scorrano, S.; Mele, G. Molecularly Imprinted Polymers: Present and Future Prospective. *Int. J. Mol. Sci.* **2011**, 12 (9), 5908–5945.

(5) Kadhirvel, P.; Azenha, M.; Shinde, S.; Schillinger, E.; Gomes, P.; Sellergren, B.; Silva, A. F. Imidazolium-based functional monomers for the imprinting of the anti-inflammatory drug naproxen: Comparison of acrylic and sol–gel approaches. *J. Chromatogr., A* **2013**, 1314, 115–123.

(6) Azenha, M.; Szefczyk, B.; Loureiro, D.; Kathirvel, P.; Cordeiro, M. N.; Fernando-Silva, A. Molecular dynamics simulations of pregelification mixtures for the production of imprinted xerogels. *Langmuir* **2011**, 27 (8), 5062–5070.

(7) Azenha, M.; Szefczyk, B.; Loureiro, D.; Kathirvel, P.; Cordeiro, M. N.; Fernando-Silva, A. Computational and experimental study of the effect of PEG in the preparation of damascenone-imprinted xerogels. *Langmuir* **2013**, 29 (6), 2024–2032.

(8) Van Der Spoel, D.; Lindahl, E.; Hess, B.; Groenhof, G.; Mark, A. E.; Berendsen, H. J. C. GROMACS: Fast, flexible, and free. *J. Comput. Chem.* **2005**, 26 (16), 1701–1718.

(9) Jorgensen, W. L.; Chandrasekhar, J.; Madura, J. D.; Impey, R. W.; Klein, M. L. Comparison of simple potential functions for simulating liquid water. *J. Chem. Phys.* **1983**, 79 (2), 926–935.

(10) Azenha, M.; Szefczyk, B.; Loureiro, D.; Kathirvel, P.; Cordeiro, M. N. D. S.; Fernando-Silva, A. Molecular Dynamics Simulations of Pregelification Mixtures for the Production of Imprinted Xerogels. *Langmuir* **2011**, 27 (8), 5062–5070.

(11) Frisch, M. J.; Trucks, G. W.; Schlegel, H. B.; Scuseria, G. E.; Robb, M. A.; Cheeseman, J. R.; Scalmani, G.; Barone, V.; Mennucci, B.; Petersson, G. A.; Nakatsuji, H.; Caricato, M.; Li, X.; Hratchian, H. P.; Izmaylov, A. F.; Bloino, J.; Zheng, G.; Sonnenberg, J. L.; Hada, M.; Ehara, M.; Toyota, K.; Fukuda, R.; Hasegawa, J.; Ishida, M.; Nakajima, T.; Honda, Y.; Kitao, O.; Nakai, H.; Vreven, T.; Montgomery, J. A., Jr., Peralta, J. E.; Ogliaro, F.; Bearpark, M.; Heyd, J. J.; Brothers, E.; Kudin, K. N.; Staroverov, V. N.; Kobayashi, R.; Normand, J.; Raghavachari, K.; Rendell, A.; Burant, J. C.; Iyengar, S. S.; Tomasi, J.; Cossi, M.; Rega, N.; Millam, J. M.; Klene, M.; Knox, J. E.; Cross, J. B.; Bakken, V.; Adamo, C.; Jaramillo, J.; Gomperts, R.; Stratmann, R. E.; Yazyev, O;

Austin, A. J.; Cammi, R.; Pomelli, C.; Ochterski, J. W.; Martin, R. L.; Morokuma, K.; Zakrzewski, V. G.; Voth, G. A.; Salvador, P.; Dannenberg, J. J.; Dapprich, S.; Daniels, A. D.; Farkas, Ö.; Foresman, J. B.; Ortiz, J. V.; Cioslowski, J.; Fox, D. J. *Gaussian 09*, revision A.02; Gaussian, Inc.: Wallingford, CT, 2009.

(12) Breneman, C. M.; Wiberg, K. B. Determining atom-centered monopoles from molecular electrostatic potentials. The need for high sampling density in formamide conformational analysis. *J. Comput. Chem.* **1990**, *11* (3), 361–373.

(13) Martinez, L.; Andrade, R.; Birgin, E. G.; Martinez, J. M. PACKMOL: A package for building initial configurations for molecular dynamics simulations. *J. Comput. Chem.* **2009**, *30* (13), 2157–2164.

(14) Hockney, R. W.; Goel, S. P.; Eastwood, J. W. Quiet high-resolution computer models of a plasma. *J. Comput. Phys.* **1974**, *14* (2), 148–158.

(15) Bussi, G.; Donadio, D.; Parrinello, M. Canonical sampling through velocity rescaling. *J. Chem. Phys.* **2007**, *126* (1), No. 014101.

(16) Parrinello, M.; Rahman, A. Polymorphic transitions in single crystals: A new molecular dynamics method. *J. Appl. Phys.* **1981**, *52* (12), 7182–7190.

(17) Nosé, S.; Klein, M. L. Constant pressure molecular dynamics for molecular systems. *Mol. Phys.* **1983**, *50* (5), 1055–1076.

(18) Jorgensen, W. L.; Maxwell, D. S.; Tirado-Rives, J. Development and Testing of the OPLS All-Atom Force Field on Conformational Energetics and Properties of Organic Liquids. *J. Am. Chem. Soc.* **1996**, *118* (45), 11225–11236.

(19) Essmann, U.; Perera, L.; Berkowitz, M. L.; Darden, T.; Lee, H.; Pedersen, L. G. A smooth particle mesh Ewald method. *J. Chem. Phys.* **1995**, *103* (19), 8577–8593.

(20) Humphrey, W.; Dalke, A.; Schulten, K. VMD: Visual molecular dynamics. *J. Mol. Graphics* **1996**, *14* (1), 33–38.

(21) Pereira, J. C. G.; Catlow, C. R. A.; Price, G. D. Molecular Dynamics Simulation of Liquid H₂O, MeOH, EtOH, Si(OMe)₄, and Si(OEt)₄, as a Function of Temperature and Pressure. *J. Phys. Chem. A* **2001**, *105* (10), 1909–1925.

(22) Pereira, J. C. G.; Catlow, C. R. A.; Price, G. D. Molecular Dynamics Simulation of Methanolic and Ethanolic Silica-Based Sol-Gel Solutions at Ambient Temperature and Pressure. *J. Phys. Chem. A* **2002**, *106* (1), 130–148.

(23) Gohlke, H.; Thorpe, M. F. A natural coarse graining for simulating large biomolecular motion. *Biophys. J.* **2006**, *91* (6), 2115–2120.

(24) Ruymgaart, A. P.; Elber, R. Revisiting Molecular Dynamics on a CPU/GPU System: Water Kernel and SHAKE Parallelization. *J. Chem. Theory Comput.* **2012**, *8* (11), 4624–4636.